POLISH MARITIME RESEARCH 1 (129) 2026 Vol. 33; pp. 99-106
10.2478/pomr-2026-0009

Evaluation of the Efficiency and Strength Analysis of Profiled Heating Surfaces with Controlled Flow Separation in Marine Waste Heat Recovery Boilers

Svitlana Kuznetsova [1]
Dmytro Lytvynenko *
Valerii Kuznetsov *
Admiral Makarov National University of Shipbuilding, Mykolaiv, Ukraine

* Corresponding author: *valeriy.kuznetsov@nuos.edu.ua (Valerii Kuznetsov)*

ABSTRACT

The utilisation of exhaust gas heat from diesel engines is one of the most effective ways to improve the performance of marine power plants. Achieving the same boiler performance, given the reduction in the exhaust gas temperature resulting from increased engine thermal efficiency, has led to an increase in boiler dimensions and has complicated their installation within the exhaust gas ducts of power plants. To reduce these parameters, the efficiency of using elliptical heating surfaces with a controlled flow separation mechanism in the form of a triangular notch has been considered for the intensification of heat transfer processes. It was found that for a main engine power of about 10,000 kW, the steam production rate of the waste heat recovery boiler can reach up to 3,000 kg/h, which is sufficient to fully meet the steam demand under cruising conditions or to significantly reduce the load on the auxiliary boiler. A strength analysis of the elliptical surfaces was carried out to determine the required wall thickness. The wall thickness must ensure that the surface retains its shape under an internal pressure of no less than 0.7 MPa. The analysis was performed using the finite element method. Verification was conducted by comparing the results with available experimental data. The results showed that, depending on the internal pressure, the pipe wall thickness should be within the range of 1 to 2 mm. According to the strength requirements, the pipe material must comply with AISI A 283-C, A516-55, or A182 Grade F12.

Keywords: marine power plants, waste heat recovery boiler, profiled heating surface, internal pressure, equivalent stresses

INTRODUCTION

A current requirement for modern marine power plants is ensuring both their environmental and economic efficiency [1]. To monitor compliance with these requirements, the International Maritime Organization (IMO) has developed and implemented the following indicators: the Energy Efficiency Design Index (EEDI) for newly built ships, the Energy Efficiency Existing Ship Index (EEXI), and the Carbon Intensity Indicator (CII) for ships in operation [2, 3, 4].

A distinctive feature of the first two indicators is that they account only for emissions from thermal engines that produce mechanical work – namely, the main and auxiliary engines – while excluding emissions from the auxiliary boiler. The third indicator, on the other hand, considers all emissions from the ship's power plant, including those from the main and auxiliary engines, as well as the auxiliary boiler. For bulk carriers, general cargo ships, and container vessels, the steam demand typically does not exceed 5,000 kg/h, and therefore the efficiency assessment of an operating vessel can be performed using the EEXI. For these types of vessels, auxiliary boilers typically do not operate during sea voyages, and the steam demand is primarily covered by the waste-heat boilers. However, for tankers, which may include up to two auxiliary fired boilers with a steam production capacity of 10,000 to 16,000 kg/h of saturated steam each, the evaluation of environmental and economic efficiency is more appropriately carried out using the CII. It should also be noted that, according to the order book for 2022–2024, oil tanker orders accounted for approximately 22% of orders. An important role in this segment is played by tankers with a deadweight of 45,000–50,000 tons [5, 6].

According to the CII, improving the environmental efficiency of a vessel can be achieved by reducing the fuel consumption of the ship's power plant. It is well known that one of the most effective methods used to accomplish this is the utilisation of exhaust gas heat from the main and auxiliary engines.

However, the following should be taken into account. The improvement of low-speed main marine diesel engines has reduced the potential for exhaust gas heat recovery due to the decrease in the exhaust gas temperature.

For example, on tankers with a deadweight of 45,000–50,000 tons, engines such as the 6S50ME and 6G50ME may be used according to the data presented in [5]. Fig. 1 shows a comparative assessment of the available exhaust gas heat flow rates for these engines. The calculation was performed using the CEAS online engine calculation service under ISO conditions (ambient temperature of 25 °C, cooling water temperature of the charge air cooler of 25 °C) at an operating power of Ne = 9,690 kW [7].

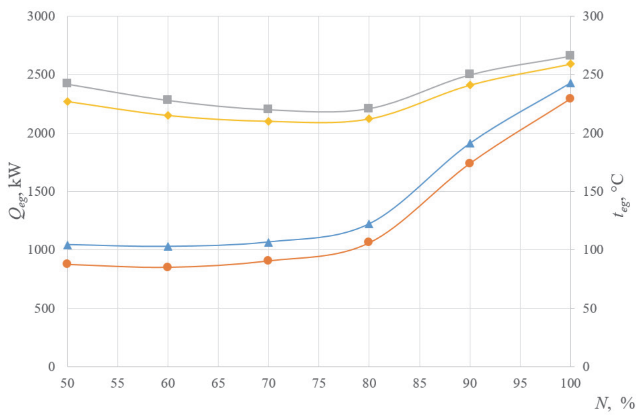

Fig. 1. Dependence of available exhaust gas heat flow rate (Q_{eg}) and exhaust gas temperature (t_{eg}) on relative engine load (N): ■,♦ – exhaust gas temperatures of the 6S50ME and 6G50ME engines, respectively, °C; ▲,● – available exhaust gas heat flow rates of the 6S50ME and 6G50ME engines, respectively

The analysis of the obtained results shows that, for the 6G50ME engine, compared to the 6S50ME engine, within the load range of 0.5…1.0 N, the reduction in the available exhaust gas heat flow rate at each load point is 5…12%, which will significantly complicate the recovery of the waste heat.

Thus, the development of efficient waste heat recovery systems for marine power plants is an urgent and relevant problem. Its implementation will help reduce harmful emissions into the environment and improve the technical and economic efficiency of marine power plants by decreasing the overall fuel consumption of the system.

LITERATURE ANALYSIS OF EXISTING TECHNICAL SOLUTIONS AND FORMULATION OF RESEARCH OBJECTIVES

To date, a large number of methods and corresponding system configurations have been proposed for the recovery of exhaust gas heat from main and auxiliary engines.

In [8, 9], it has been proposed to utilise the low-grade heat of exhaust gases from marine thermal engines in thermoacoustic systems for electricity generation. However, the application of such systems is limited by the need to install a considerable amount of additional equipment within the confined spaces of engine rooms, their relatively low power output, and their dependence on the characteristics of internal heat exchangers.

An original method for exhaust gas heat recovery was proposed by the authors of [10]. The article presents the results of an analysis of the effect obtained from cooling the air at the inlet of an engine turbocharger using thermally driven refrigeration machines that utilise the heat of exhaust and recirculated (environmental) gases. It is shown that inlet air cooling in ejector and absorption refrigeration systems can significantly reduce the specific fuel consumption of the engine. However, further research is required to investigate the effect of the air temperature at the engine cylinder inlet after the refrigeration machines on the thermal state of diesel engine components.

In [11], the issues of exhaust gas heat recovery from internal combustion engines operating on water-fuel emulsions are considered. The results presented include an analysis of the mechanism of deposit formation from exhaust gases on the condensation heat transfer surface of an economiser and an evaluation of their influence on the heat and mass transfer characteristics of waste heat recovery boilers. The applicability of the presented results is limited by the restricted use of water-fuel emulsions in marine diesel power plants and by the need for further investigation of the heat and mass transfer processes in steam-gas mixtures under the given conditions.

In [12, 13], it has been proposed to utilise the heat of exhaust gases to implement thermochemical heat recovery technologies in marine power plants. It has been shown that thermochemical technologies have significant potential for expanding the range of alternative fuels and can be applied in various configurations of hybrid marine power systems. However, the obtained results require further investigation, as they were derived under operating conditions specific to gas turbine power plants.

The traditional method of utilising exhaust gas heat from main and auxiliary engines involves the use of waste heat recovery boilers. The steam generated in such systems is employed for general shipboard or specialised needs, or in waste heat recovery turbogenerators [14, 15, 16].

However, the reduction in the energy potential of exhaust gases has made the implementation of such systems more difficult. Despite the trend toward a gradual decrease in sulphur content in marine fuels [17] and the corresponding possibility of lowering the exhaust gas temperature at the outlet of the waste heat recovery boiler [18], according to the assessment presented in [19], the transition from MAN B&W S-series engines to G-series engines may increase the required boiler surface area by up to 33%. This, in turn, complicates its installation within the engine room casing.

To reduce the weight and size parameters of waste heat recovery boilers, heat transfer intensification methods are applied. For this purpose, various types of finned surfaces are commonly used, including spiral-strip fins, disc-type fins, H-type fins, segmented fins, and fins with bent edges mounted on round or flat-oval carrier tubes [16, 18, 20, 21, 22]. Despite their evident advantages, finned surfaces also have significant drawbacks – increased aerodynamic resistance and a tendency for the heating surfaces to become contaminated.

The study [19] substantiated the prospects of using smooth elliptical tubes with a controlled flow separation mechanism as heating surfaces in marine waste heat recovery boilers. To further justify the effectiveness of their application, it is advisable to evaluate their steam generation capacity as a function of the main engine power, as well as to determine the maximum internal pressure that the elliptical surface can withstand without deformation.

INVESTIGATION METHOD

The steam generation rate of the waste heat recovery boiler was adopted as the indicator of its efficiency. A comparative calculation was performed for the 6S50ME and 6G50ME engines using the online service [7] at a power output of 9,690 kW for a waste heat recovery boiler heating surface made of smooth round tubes. For the calculation of the heating surface composed of elliptical tubes with a controlled flow separation mechanism, the results of [19] were used.

Since the ratio of the wall thickness to the inner diameter of the tube, as an element of the heat exchange surface, was not less than 1/20, it was considered a thick-walled cylinder for subsequent calculations [23, 24].

In this case, the tube is simultaneously subjected to the uniformly distributed internal pressure Pw from the water and forces induced by the gas flow acting on its outer surface. In addition, the tube operates under high-temperature conditions. The stress–strain state at any point of such a tube represents a superposition of the effects produced by the aforementioned loads.

It is evident that the stresses in the tube caused by the gas flow are considerably less significant than those resulting from the internal water pressure; therefore, they can be neglected.

Thermal stresses were also not taken into account. This is due to the fact that the temperatures on the outer and inner surfaces of the tube are comparable in magnitude, and the supports at the ends of the cylinder are movable.

The problem of determining the stress field in the cross-section of such a tube can be considered a plane problem. Neglecting thermal stresses and body forces, the following differential equilibrium equations for a two-dimensional case can be written in accordance with [23]:

$$\left.\begin{aligned}\frac{\partial\sigma_x}{\partial x}+\frac{\partial\tau_{xy}}{\partial y}=0,\\ \frac{\partial\sigma_y}{\partial y}+\frac{\partial\tau_{xy}}{\partial x}=0,\end{aligned}\right\} \tag{1}$$

where σ_x and σ_y are the components of the normal stresses at a point in the body acting along the corresponding axes, and τ_{xy} is the shear stress at that point.

The presented differential equations must satisfy the boundary conditions on the surface of the body, which are expressed as follows:

$$\left.\begin{aligned}X_\nu=\sigma_x l+\tau_{xy}m,\\ Y_\nu=\tau_{yx}l+\sigma_y m,\end{aligned}\right\} \tag{2}$$

where X_ν and Y_ν are the components of the surface forces parallel to the coordinate axes *Ox* and *Oy*, and *l* and *m* are the direction cosines of the normal to the boundary.

The system of equations (1) must be complemented by the strain compatibility equation:

$$\frac{\partial^2\varepsilon_x}{\partial y^2}+\frac{\partial^2\varepsilon_y}{\partial x^2}=\frac{\partial^2\gamma_{xy}}{\partial x\partial y} \tag{3}$$

where ε_x and ε_y are the components of linear strain along the *Ox* and *Oy* axes, and γ_{xy} is the component of shear strain.

The strain components in Eq. (3) are related to the stress components according to Hooke's law [23].

The method for solving the previously presented equations of the theory of elasticity for the plane problem involves introducing a new function – the stress function $\varphi(x, y)$. In the absence of body forces, the stress function is related to the stress components by the following relationships:

$$\sigma_x=\frac{\partial^2\varphi}{\partial y^2}, \sigma_y=\frac{\partial^2\varphi}{\partial x^2}, \tau_{xy}=-\frac{\partial^2\varphi}{\partial x\partial y}. \tag{4}$$

Reference [23] presents a solution to Eqs. (1)–(3) that describes the stress field in a hollow cylinder subjected to uniform pressure on its inner and outer surfaces. To determine the stress field in cross-sections of more complex geometries, it is advisable to employ numerical methods.

According to [23], a tube subjected to internal pressure experiences the following stress components: the principal stress acting orthogonally to the plane containing the axis of symmetry of the cylinder, referred to as the circumferential (hoop) stress σθ; the principal stress acting orthogonally to the transverse section, referred to as the longitudinal stress σz; and the principal stress acting orthogonally to the plane tangent to the cylindrical surface, referred to as the radial stress σr (Figs. 2 and 3).

a

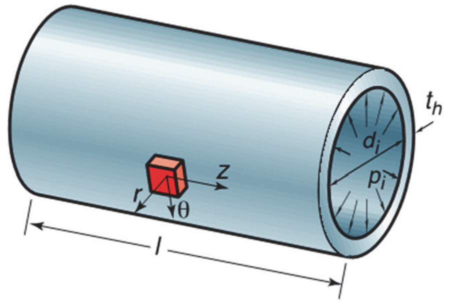

b

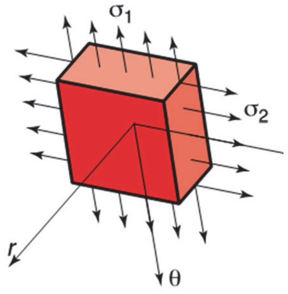

Fig. 2. Thick-walled cylinder as an element of a tube with a circular cross-section subjected to internal pressure: (a) schematic representation of the cylinder; (b) cylinder element and the stresses acting on it

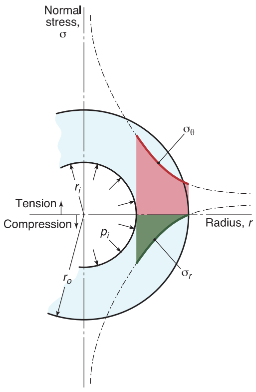

Fig. 3. Stresses in a thick-walled cylinder subjected to internal pressure

To determine the stress field in a cylinder with a circular cross-section, it is necessary, according to [24], to transition from a Cartesian coordinate system to a polar coordinate system centred at the intersection point of the diagonals of the opening. In the polar coordinate system, assuming that body forces are equal to zero, the stress components can be expressed as follows:

$$\sigma_r = \frac{1}{r}\frac{\partial\varphi}{\partial r} + \frac{1}{r^2}\frac{\partial^2\varphi}{\partial\theta^2},\ \sigma_\theta = \frac{\partial^2\varphi}{\partial r^2},\ \tau_{r\theta} = -\frac{\partial}{\partial r}\left(\frac{1}{r}\frac{\partial\varphi}{\partial\theta}\right), \quad (5)$$

When determining the stress field in a cylinder with a circular cross-section, the stress function φ(*r*, *θ*) in polar coordinates depends only on the magnitude of the radius vector *r*. It can be expressed by the following formula:

$$\varphi = A \cdot lnr + Br^2 lnr + Cr^2 + D, \quad (6)$$

where *A*, *B*, *C*, and *D* are constants.

The corresponding stress components can be obtained by substituting Eq. (2) into Eq. (1); in this case, they take the following form:

$$\begin{gathered} \sigma_r = \frac{1}{r}\frac{\partial\varphi}{\partial r} = \frac{A}{r^2} + B(1+2lnr) + 2C, \\ \sigma_\theta = \frac{\partial^2\varphi}{\partial r^2} = -\frac{A}{r^2} + B(3+2lnr) + 2C, \\ \tau_{r\theta} = 0 \end{gathered} \quad (7)$$

For a cylinder with a circular cross-section, it can be assumed in Eq. (7) that *B* = 0, according to [24]. The boundary conditions of the problem, when only the internal pressure p_i acts on such a cylinder, are as follows:

$$(\sigma_r)_{r=r_i} = -p_i;\ (\sigma_r)_{r=r_0} = 0, \quad (8)$$

where r_i is the inner radius of the tube and r_o is the outer radius of the tube.

After substituting Eq. (8) into Eq. (7), the following expressions for the radial and hoop stresses in a cylinder subjected to internal pressure pi can be obtained:

$$\sigma_r = \frac{p_i r_i^2\left(1-\frac{r_o^2}{r^2}\right)}{r_o^2 - r_i^2}, \quad (9)$$

$$\sigma_\theta = \frac{p_i r_i^2\left(1+\frac{r_o^2}{r^2}\right)}{r_o^2 - r_i^2} \quad (10)$$

where r_i is the inner radius of the tube, r_o is the outer radius of the tube, and *r* is the radius vector of the point under consideration.

To verify the strength condition, the third or fourth strength hypothesis can be applied, assuming that the material is ductile (steel) [23].

According to the third strength hypothesis, the strength condition is expressed as follows:

$$\sigma_\theta - \sigma_r \leq [\sigma]. \quad (11)$$

According to the fourth strength hypothesis, assuming that longitudinal stresses are not included in the calculation, the strength condition is as follows:

$$\frac{\sqrt{2}}{2}\sqrt{(\sigma_r - \sigma_\theta)^2 + {\sigma_\theta}^2 + {\sigma_r}^2} \leq [\sigma]. \quad (12)$$

Thus, the equivalent stresses, in accordance with relation (12), are determined by the following expression:

$$\sigma_{eqv} = \frac{\sqrt{2}}{2}\sqrt{(\sigma_r - \sigma_\theta)^2 + {\sigma_\theta}^2 + {\sigma_r}^2}. \quad (13)$$

The shape of the elliptical tube cross-section is shown in Fig. 4. For the calculations, a cylindrical coordinate system was adopted, with its centre located at the intersection point of the ellipse's symmetry axes. In evaluating the tube's strength, only the circumferential and radial stresses and their distribution over the cross-section were determined. The stresses acting along the longitudinal axis were not taken into account.

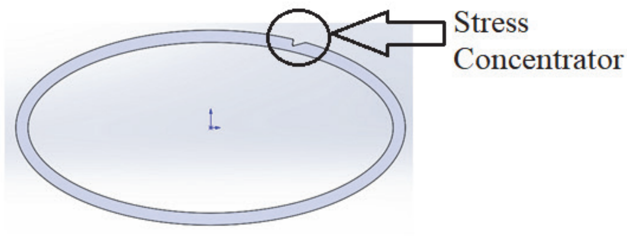

Fig. 4. Cross-sectional shape of the tube

The triangular notch was considered the critical point in the cross-section, acting as a stress concentrator and representing the most probable location of the maximum equivalent stress. This geometric feature was assumed to govern the onset of local plastic deformation and, consequently, to determine the overall strength reliability of the elliptical tube section.

Considering the complexity of the cross-sectional geometry of the specimen with a triangular notch acting as a stress concentrator, the finite element method (FEM) was chosen to study the stress field [25, 26, 27]. The general finite element equation for a system consisting of an arbitrary number of elements, in which the primary unknowns are the displacements, is expressed as follows:

$$\{F\} = [K]\{U\}, \tag{14}$$

where $[K]$ is the global stiffness matrix of the entire model; $\{U\}$ is the global nodal displacement vector, which represents the unknown quantities; and $\{F\}$ is the global nodal force vector for the entire model.

The finite element model of the cylindrical element is shown in Fig. 5a, and the mesh discretisation in the region of the stress concentrator is shown in Fig. 5b. The element length was selected to minimise the influence of the symmetry boundary conditions at the cylinder ends on the stress distribution diagram in the midsection of the tube. The internal pressure was applied perpendicular to the inner surface of the tube.

a

b

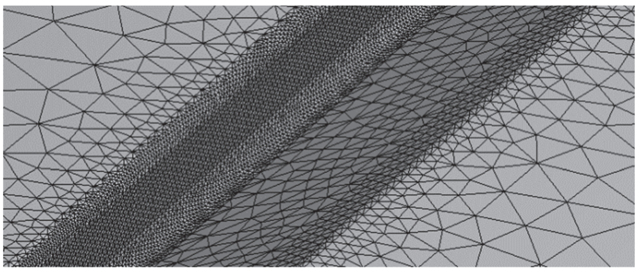

Fig. 5. (a) Finite element model and (b) mesh discretisation near the stress concentrator

The verification and validation of the adopted computational model were carried out using a tube with a circular cross-section, for which well-known theoretical solutions exist [23]. The outer diameter of this tube was 16 mm, and the inner diameter was 14 mm. The element length of this tube was the same – 50 mm. The boundary conditions at the bar ends were also identical.

The finite element calculation results for the circumferential and radial stresses of the previously described circular tube element are presented in Figs. 6 and 7, respectively, in a cylindrical coordinate system. The internal pressure was 1 MPa. The material used was AISI A201 GrAFx at a temperature of 20 °C. The mechanical properties of the material were taken from [28].

According to Eq. (5), the radial stresses reach their maximum value of 1 MPa on the inner surface of the tube under an internal pressure of 1 MPa. The same results were obtained using the finite element method. The circumferential stresses also reach their maximum on the inner surface of the tube; according to Eq. (6), their value should be 7.53 MPa. This value was likewise confirmed by the finite element calculations. Thus, the adopted boundary conditions make it possible to obtain results that are consistent with the analytical solution.

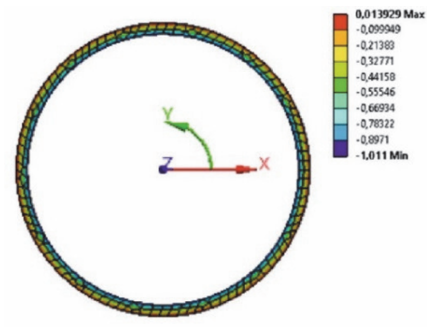

Fig. 6. Distribution of radial stresses in the tube with a circular cross-section

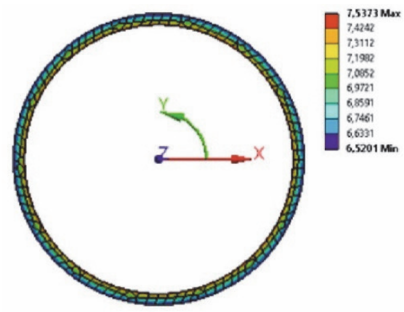

Fig. 7. Distribution of hoop stresses in the tube with a circular cross-section

RESULTS OF THE STUDY

According to the data presented in [5, 29, 30], the total steam consumption, kg/hour, at a pressure of 0.7 MPa for tankers with a deadweight of approximately 50,000 tons is as follows:

- ballast crossing: 1,800–2,200;
- voyage with cargo temperature maintenance: 5,500–5,800;
- voyage with cargo heating: 13,100–13,600;
- passage with mopping up of tanks: 11,700–12,100.

The steam demand is met by the operation of both the waste heat recovery boiler and the auxiliary boiler of the boiler plant. The steam generation rate of the waste heat recovery boiler usually does not exceed 1,000 kg/h. Therefore, in certain operating modes, additional steam must be supplied by the auxiliary boiler, which increases fuel consumption and reduces overall system efficiency.

The results of the comparative analysis of the waste heat recovery boiler steam generation rate are presented in Fig. 8. The results were obtained on the basis of [7] and [19].

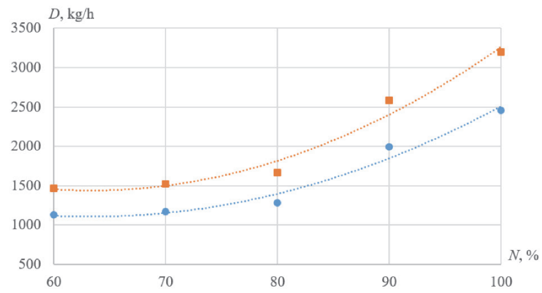

a

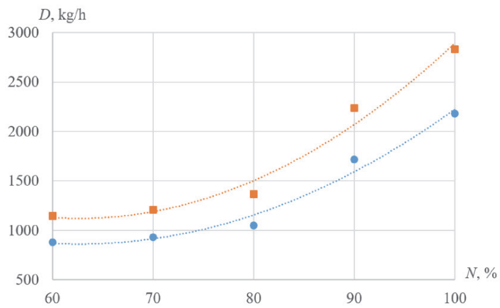

b

Fig. 8. Results of the calculation of the waste heat recovery boiler steam generation rate for the (a) 6S50ME and (b) 6G50ME engines at a nominal power of Ne = 9690 kW: ● – steam generation rate of the boiler with a circular heating surface; ■ – steam generation rate of the boiler with an elliptical heating surface featuring controlled flow separation

For the 6S50ME engine, within the range of 75–90% of the nominal power, the steam generation rate of the waste heat recovery boiler does not exceed 1,990 kg/h. Under certain external operating conditions, this may necessitate the use of the auxiliary boiler at a very low load to meet the vessel's steam demand during the ballast voyage mode. With the use of elliptical heating surfaces with controlled flow separation in waste heat recovery boilers, the steam demand in this operating mode can be almost completely satisfied, while the load on the auxiliary boiler is significantly reduced under other operating conditions.

For the 6G50ME engine, within the range of 75–90% of the nominal power, the use of elliptical heating surfaces with controlled flow separation in waste heat recovery boilers makes it possible – due to a reduction in the exhaust gas temperature of 8–10 °C – to almost fully satisfy the vessel's steam demand under ballast voyage conditions, depending on external operating factors, and to reduce the load on the auxiliary boiler under other vessel operating modes.

Overall, the application of elliptical heating surfaces provides a 10–15% improvement in steam generation efficiency and ensures a more stable boiler performance across different operating modes.

The results of the finite element analysis of equivalent stresses, calculated using Eq. (9), are presented in Figs. 9 and 10 for the stress concentration region – the triangular notch, where the highest stress values were obtained as a result of the simulation.

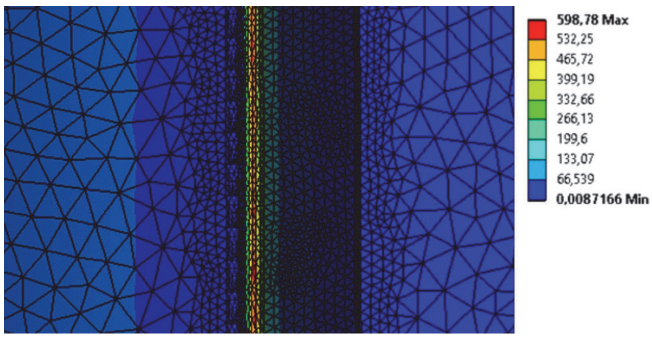

Fig. 10. Distribution of equivalent stresses within the stress concentrator of the elliptical tube with a longitudinal notch

As can be seen from Figs. 9 and 10, the equivalent stresses in the stress concentrator significantly exceed the yield strength of the material (for AISI A201, GrAFx $\sigma_T \approx 225$ MPa). Considering that the stress calculations were performed under the assumption of a linear relationship between stresses and strains, it can be concluded that the strength of such a tube will be ensured only at an internal pressure not exceeding 0.25 MPa.

Significant values of the equivalent stresses σ_{eqv} were also observed in the region of the major axis of the elliptical

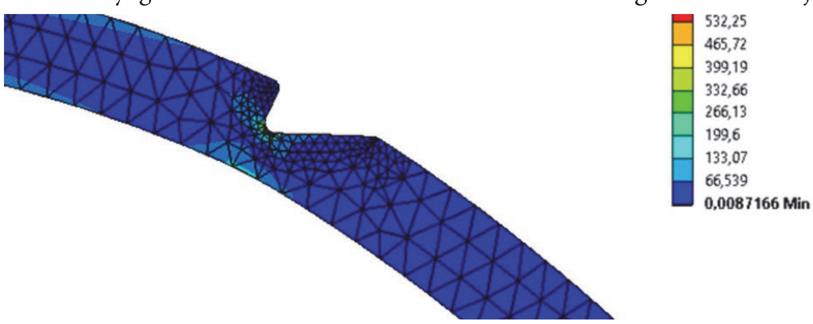

Fig. 9. Distribution of equivalent stresses in the area of the stress concentrator within the cross-section of the elliptical tube with a longitudinal notch

cross-section, on its inner surface, as shown in Fig. 11. This stress distribution is determined by the geometry of the tube cross-section. The equivalent stresses in this region reached the level of the steel's yield strength. To ensure the structural integrity of the tube in this area, it is necessary to use steels with stronger mechanical properties. In addition, the wall thickness of the tube can be increased or the cross-sectional profile shape can be modified to reduce stress levels.

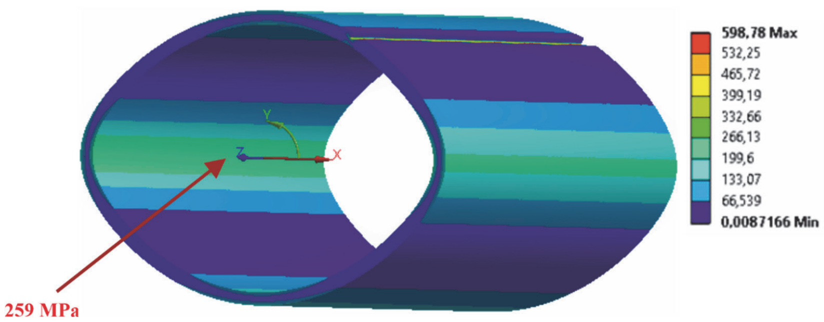

Fig. 11. Equivalent stresses in the region of the major axis of the elliptical tube with a longitudinal notch

DISCUSSION OF RESULTS

The increase in the efficiency of main marine engines and the reduction in the energy potential of their exhaust gases have limited the possibilities for waste heat recovery. A promising approach to implementing the waste heat recovery process is the use of waste heat recovery boilers with elliptical heat exchange surfaces featuring controlled flow separation.

The results of the efficiency assessment demonstrate that such boilers can fully supply the steam demand of the ship's power plant under propulsion conditions, where the steam consumption does not exceed 3,000 kg/h. Under other operating modes, the use of this design allows a significant reduction in the load on the auxiliary boiler of the ship's power plant.

The use of elliptical heating surfaces has its own specific features. This is due to the presence of internal pressure in the tube, which tends to restore the elliptical cross-section to a circular shape. To prevent this effect, the wall thickness of a smooth elliptical tube should be at least 1.0–1.5 mm, and for a smooth elliptical tube with controlled flow separation, it should be 1.5–2.0 mm. An alternative solution is the use of steels with stronger mechanical properties, such as AISI A283-C, A516-55, or A182 Grade F12.

It is advisable to conduct further research on the shape of the notch used for flow separation control in order to reduce the equivalent stresses while maintaining the achieved thermo-hydraulic characteristics.

CONCLUSION

1. The use of elliptical heat exchange surfaces with controlled flow separation in the waste heat recovery boilers of tankers with a deadweight of 45,000–50,000 tons can make it possible to meet the steam demand of the ship's power plant during the ballast voyage mode, as well as significantly reduce the load on the auxiliary boiler plant under other operating conditions.

2. The finite element analysis of the stress–strain state of an elliptical tube with a triangular cutout used for flow separation control showed that the highest stresses occur in the flow separation control element – the triangular notch. These stresses significantly exceed the yield strength of the investigated material, AISI A201 GrAFx steel. High stress levels were also observed in the region of the major axis of the elliptical tube cross-section.

3. To ensure the strength of the tube material under the specified levels of internal pressure and temperature, one could use steels with stronger mechanical properties, optimise the shape of the notch to reduce the stress concentration, or increase the wall thickness of the tube.

REFERENCES

1. MARPOL Annex VI and the Act to Prevent Pollution from Ships (APPS). Retrieved from https://www.epa.gov/enforcement/marpol-annex-vi-and-act-prevent-pollution-ships-apps.

2. ANNEX 9: Resolution MEPC.364(79) – 2022 Guidelines on the Method of Calculation of the Attained Energy Efficiency Design Index (EEDI) for New Ships. Retrieved from https://wwwcdn.imo.org/localresources/en/KnowledgeCentre/IndexofIMOResolutions/MEPCDocuments/MEPC.364(79).pdf.

3. ANNEX 12: Resolution MEPC.350(78) – 2022 Guidelines on the Method of Calculation of the Attained Energy Efficiency Existing Ship Index (EEXI) (Adopted on 10 June 2022). Retrieved from https://www.mardep.gov.hk/filemanager/en/share/msnote/pdf/msin2302anx6.pdf.

4. ANNEX 10: Resolution MEPC.336(76) (adopted on 17 June 2021). 2021 guidelines on operational carbon intensity indicators and the calculation methods (CII Guidelines, G1). Retrieved from https://wwwcdn.imo.org/localresources/en/KnowledgeCentre/IndexofIMOResolutions/MEPCDocuments/MEPC.336(76).pdf.

5. Significant Ships 2014–2024. Retrieved from https://www.libramar.net/news/significant_ships_series/1-0-140.

6. UNCTAD: Review of maritime transport 2024. Retrieved from https://unctad.org/publication/review-maritime-transport-2024.

7. MAN Energy Solutions: CEAS Engine Calculations. Retrieved from https://www.everllence.com/

marine/products/planning-tools-and-downloads/ceas-engine-calculations/.

8. Korobko V., Serbin S. and Le H. Exploration of a model thermoacoustic turbogenerator with a bidirectional turbine. Polish Maritime Research, 2023. https://doi.org/10.2478/pomr-2023-0063.

9. Korobko V., Shevtsov A., Serbin S., Wen H. and Dzida M. Impact of the type of heat exchanger on the characteristics of low-temperature thermoacoustic heat engines. International Journal of Thermofluids, 2024. https://doi:10.1016/j.ijft.2024.100953.

10. Pyrysunko M., Radchenko R., Kornienko V. and Shalapko D. Analysis of cooling air at the inlet of marine engine with exhaust gas recirculation by ejector and absorption refrigeration. In: Lecture Notes in Mechanical Engineering: Proceedings of the 7th International Conference on Design, Simulation, Manufacturing: The Innovation Exchange (DSMIE 2024), Pilsen, Czech Republic, 4–7 June 2024, pp. 314–323. https://doi:10.1007/978-3-031-63720-9_27.

11. Kornienko V., Radchenko M., Radchenko R., Pavlenko A. and Radchenko A. A new trend in combustion engine's deep waste heat recovery by application of condensing economizers in exhaust boilers. Applied Thermal Engineering, 2025, vol. 261. https://doi: 10.1016/j.applthermaleng.2024.125150.

12. Cherednichenko O., Serbin S., Tkach M., Kowalski J. and Chen D. Mathematical modelling of marine power plants with thermochemical fuel treatment. Polish Maritime Research, 2022, vol. 29, no. 3, pp. 99–108. https://doi:10.2478/pomr-2022-0030.

13. Cherednichenko O., Serbin S., Patlaichuk V., Lychko B. and Ratushniak I. Utilizing thermochemical waste heat recovery modules in marine hybrid power systems. In: Transport Means – Proceedings of the 27th International Scientific Conference on Transport Means 2023, Palanga, Lithuania, 4–6 October 2023, pp. 628–632. doi: 10.5755/e01.2351-7034.2023.P2

14. Singh D. and Pedersen E. A review of waste heat recovery technologies for maritime applications. Energy Conversion and Management, 2016, vol. 111, pp 315–328. https://doi:10.1016/j.enconman.2015.12.073.

15. Hoang A. Waste heat recovery from diesel engines based on organic Rankine cycle. Applied Energy, 2018, vol. 231, pp. 138–166. https://doi: 10.1016/j.apenergy.2018.09.022.

16. MAN Diesel & Turbo: Waste Heat Recovery System (WHRS) for Reduction of Fuel Consumption, Emissions and EEDI. Retrieved from https://mandieselturbo.com/docs/librariesprovider6/technical-papers/waste-heat-recovery-system.pdf.

17. Reduced Limit on Sulphur in Marine Fuel Oil Implemented Smoothly Through 2020. Retrieved from https://www.imo.org/en/MediaCentre/PressBriefings/pages/02-IMO-2020.aspx.

18. Baehr H. and Stephan K. Heat and Mass Transfer. Springer, 2021. https://doi:10.1007/978-3-642-20021-2.

19. Kuznetsov V. and Kuznetsova S. Increasing the economic efficiency of marine power plants using waste heat boilers with controlled flow separation. Polish Maritime Research, 2024. https://doi.org/10.2478/pomr-2024-0039.

20. Thulukkanam K. Heat Exchangers. Volume I: Classification, Selection, and Thermal Design. 3rd ed. Boca Raton, FL: CRC Press, 2024. https://doi: 10.1201/9781003352044.

21. Zhukova Yu., Terekh A., Isaev S. and Pismenny E. Aerodynamic and heat transfer characteristics of an oval-shaped tube at different Reynolds numbers. Heat Transfer Research, 2020, vol. 51, no. 15, pp. 1383–1397. https://doi:10.1615/HeatTransRes. 2020035821.

22. Pismenny E. Heat Transfer and Aerodynamics of Cross-Finned Tube Packages (in Russian). Kyiv, Ukraine: Altpres, 2004.

23. Timoshenko S. and Goodier J. Theory of Elasticity. 2nd ed., New York: McGraw-Hill, 1951.

24. Davis J. Tensile Testing. 2nd ed., Materials Park. OH: ASM International, 2004.

25. Patankar S. Numerical Heat Transfer and Fluid Flow. New York: Hemisphere Publishing Corporation, 1980.

26. Moaveni S. Finite Element Analysis: Theory and Application with ANSYS. Upper Saddle River. NJ: Prentice-Hall Inc., 1999.

27. Structures and Thermomechanics Analysis for Studies and Research. Retrieved from https://code-aster.org/spip.php?rubrique2

28. AISI Carbon Steel Mechanical Characteristics: Table Chart, Yield, Tensile, Hardness. Retrieved from www.engineersedge.com/materials/carbon-steel-properties1.htm.

29. Yang Z., Wen H., Yang X., Gorbov V., Mitienkova V. and Serbin S. Marine Power Plant, 2021. https://doi:10.1007/978-981-33-4935-3.

30. 17012-360.064.345Г. Fuel, Lubricating Oil and Boiler Water Reserves. Steam Balance of the Boiler Plant. Calculations (in Russian). Mykolaiv, Ukraine: UkrCDB BSP, 1993.